Elasticity of individual protocadherin 15 molecules implicates tip links as the gating springs for hearing

Tobias F. Bartsch[a,b,1], Felicitas E. Hengel[a,b,2], Aaron Oswald[a,b,2], Gilman Dionne[c], Iris V. Chipendo[a,b], Simranjit S. Mangat[a,b], Muhammad El Shatanofy[a,b], Lawrence Shapiro[c], Ulrich Müller[d], and A. J. Hudspeth[a,b,1]

[a]Howard Hughes Medical Institute, The Rockefeller University, New York, NY 10065; [b]Laboratory of Sensory Neuroscience, The Rockefeller University, New York, NY 10065; [c]Department of Biochemistry and Molecular Biophysics, Zuckerman Mind Brain Behavior Institute, Columbia University, New York, NY 10032; and [d]The Solomon Snyder Department of Neuroscience, Johns Hopkins University, Baltimore, MD 21205

Contributed by A. J. Hudspeth, March 29, 2019 (sent for review February 6, 2019; reviewed by Carlos Bustamante and Pascal Martin)

Hair cells, the sensory receptors of the inner ear, respond to mechanical forces originating from sounds and accelerations. An essential feature of each hair cell is an array of filamentous tip links, consisting of the proteins protocadherin 15 (PCDH15) and cadherin 23 (CDH23), whose tension is thought to directly gate the cell's transduction channels. These links are considered far too stiff to represent the gating springs that convert hair bundle displacement into forces capable of opening the channels, and no mechanism has been suggested through which tip-link stiffness could be varied to accommodate hair cells of distinct frequency sensitivity in different receptor organs and animals. Consequently, the gating spring's identity and mechanism of operation remain central questions in sensory neuroscience. Using a high-precision optical trap, we show that an individual monomer of PCDH15 acts as an entropic spring that is much softer than its enthalpic stiffness alone would suggest. This low stiffness implies that the protein is a significant part of the gating spring that controls a hair cell's transduction channels. The tip link's entropic nature then allows for stiffness control through modulation of its tension. We find that a PCDH15 molecule is unstable under tension and exhibits a rich variety of reversible unfolding events that are augmented when the Ca^{2+} concentration is reduced to physiological levels. Therefore, tip link tension and Ca^{2+} concentration are likely parameters through which nature tunes a gating spring's mechanical properties.

auditory system | entropic stiffness | hair cell | optical trap | vestibular system

Mechanically gated ion channels are ubiquitous. In addition to underlying our senses of hearing, balance, and touch, they are involved in the regulation of such processes as muscle extension, blood pressure, pulmonary inflation, and visceral distension. These channels are opened and closed through the action of gating springs, elastic elements that are tensioned by mechanical stimulation and in turn communicate stress to the molecular gates of the respective channels. Gating springs accordingly store mechanical energy and use it to regulate channels' open probabilities. For bacterial mechanoreceptors, which respond to osmotic stress, the cellular membrane itself serves as a gating spring (1). The ubiquitous Piezo channels of vertebrates extend three membrane-embedded arms that likely act as gating springs by flexing in response to membrane stretching (2, 3). Other mechanosensitive channels, such as NOMPC (TRPN1) in *Drosophila*, appear to be gated by the tension in elastic ankyrin domains (4).

Gating springs were first posited for hair cells of the vertebrate inner ear, the sensors of the auditory and vestibular systems (5–7). Each hair cell is surmounted by a hair bundle—a cluster of erect, actin-filled processes termed stereocilia—that is deflected by mechanical stimulation. However, the identity of the gating springs in these cells has remained controversial. A plausible candidate discovered soon after the gating-spring hypothesis was advanced is the tip link. Extending approximately 150 nm between the tip of each stereocilium and the side of its longest neighbor, the tip link is positioned to sense the shear between stereocilia when a hair bundle is deflected (Fig. 1 *A* and *B*) (8–10). The tip link is a dimer of parallel dimers, comprising two PCDH15 molecules joined at their amino termini to a pair of CDH23 molecules through a "handshake," whose stability depends on the presence of bound Ca^{2+} ions (Fig. 1*C*) (11).

The mechanical properties of hair bundles imply a gating-spring stiffness (12, 13) on the order of 1 $mN{\cdot}m^{-1}$ (1 pN/nm). However, electron microscopy images suggest that the tip link is relatively rigid (14), and crystallographic studies and molecular dynamics simulations of the relevant cadherins support a stiffness 50-fold greater than that measured (15). Therefore, it has been posited that most of a gating spring's elasticity resides at a tip link's two attachments, rather than within the link itself. However, it is possible that the tip link elongates in response to force by the straightening of its lateral thermal undulations, the working principle of an entropic spring (16). To clarify the identity of the hair cell's gating spring, we examined the elastic properties of a tip link protein.

Results

Mechanical Characteristics of PCDH15. The mechanical properties of a protein can be tested by tethering it between two surfaces, applying a force that pulls the surfaces apart, and measuring the protein tether's elongation (17). To directly explore the stiffness of a tip link, we used a high-precision optical trap to determine

Significance

Our hearing depends on mechanosensitive channels in hair cells of the inner ear. Experiments suggest that each channel is opened by a "gating spring," an elastic element that conveys displacement of a hair bundle to the channel. Appropriate stiffness of the gating spring permits the discrimination of different sound amplitudes; if the spring is too stiff, then a faint sound will elicit the same response as a loud sound, opening all of a cell's channels. Although the tip link—a fine molecular filament—might be the gating spring, its properties have remained controversial. Using high-precision optical tweezers, we demonstrate that the mechanical properties of a tip link protein correlate with those of a gating spring in vivo.

Author contributions: T.F.B. and A.J.H. designed research; T.F.B., F.E.H., A.O., I.V.C., S.S.M., M.E.S., and A.J.H. performed research; G.D., L.S., and U.M. contributed new reagents/analytic tools; T.F.B., F.E.H., and A.O. analyzed data; and T.F.B., F.E.H., A.O., and A.J.H. wrote the paper.

Reviewers: C.B., University of California, Berkeley; and P.M., Institut Curie.

The authors declare no conflict of interest.

[1]To whom correspondence may be addressed. Email: tbartsch@rockefeller.edu or hudspaj@rockefeller.edu.

[2]F.E.H. and A.O. contributed equally to this work.

This article contains supporting information online at www.pnas.org/lookup/suppl/doi:10.1073/pnas.1902163116/-/DCSupplemental.

Published online May 9, 2019.

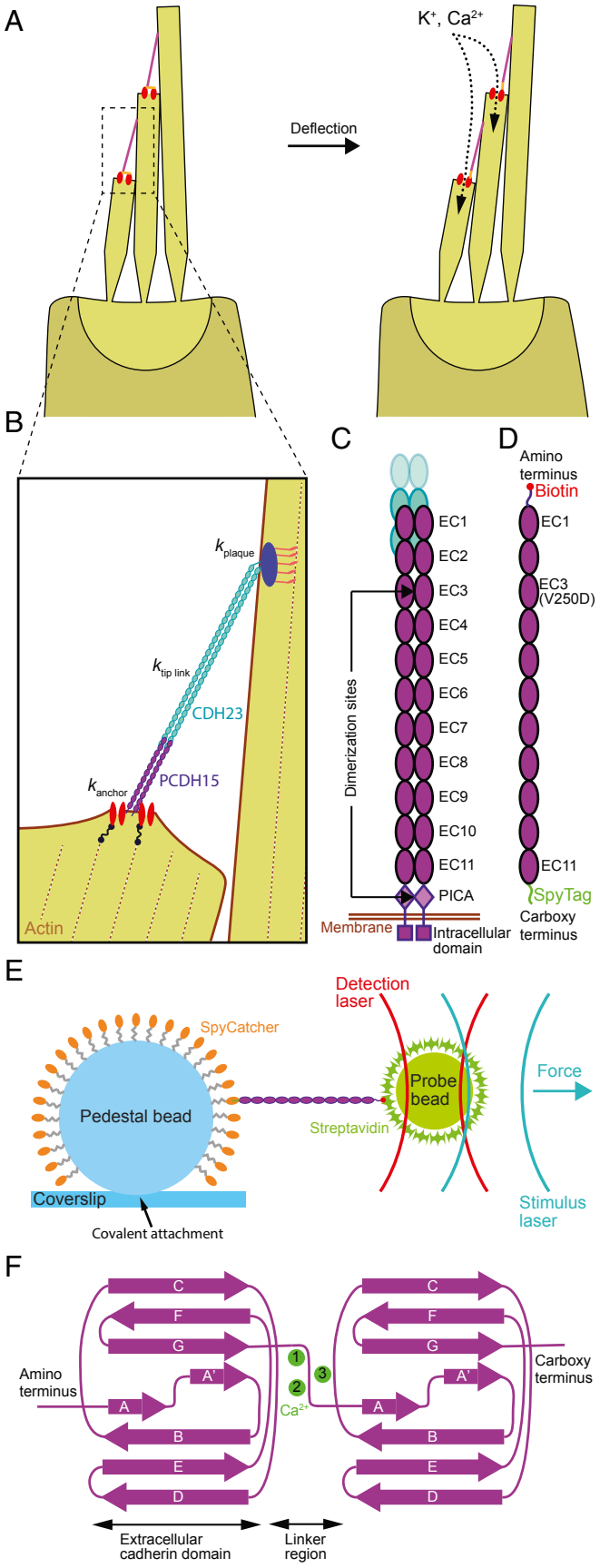

Fig. 1. The role of tip link proteins in transduction by hair cells. (*A*) The hair bundle is a cluster of stiff, actin-filled protrusions called stereocilia that stands atop each hair cell in the inner ear. Each stereocilium is connected to its tallest adjacent neighbor through a proteinaceous filament called a tip link (pink), which is coupled at its base to mechanically gated ion channels (red). Deflection of a hair bundle increases the tension in the tip links, biasing the channels toward an open state that allows the influx of positively charged ions. (*B*) The mechanical element that converts hair bundle displacement into a force capable of opening the channels is called the gating spring. Its stiffness comprises the stiffnesses of the channel and its lower anchor (k_{anchor}), the tip link proteins PCDH15 and CDH23 ($k_{tip\ link}$), and the insertional plaque that anchors the link's top end into the taller stereocilium (k_{plaque}). (*C*) The mechanical properties of the tip link emerge from its quaternary structure and from the characteristics of its constituent proteins. The lower third of the link consists of a dimer of PCDH15 molecules, each of which includes 11 extracellular cadherin (EC) domains. (*D*) To measure the mechanical behavior of monomeric PCDH15, we tagged each end with a distinct molecular handle. We eliminated dimerization by a point mutation (V250D) in domain EC3 and by truncation of the PICA domain. (*E*) We probed the mechanics of a PCDH15 monomer by confining it through molecular handles between an immobile 2-μm glass pedestal bead and a diffusive 1-μm plastic probe bead. To acquire each force-extension relationship, we measured the position of the probe bead with a detection laser while applying a force with a stimulus laser. (*F*) The folding motifs of individual EC domains influence the mechanical properties of the full-length protein. Up to three calcium ions (green) can bind between successive domains.

the mechanical properties of individual molecules of PCDH15. The extracellular portion of PCDH15 consists of 11 extracellular cadherin domains (EC1–EC11), followed by the membrane-proximal PICA domain. PCDH15 forms a homodimer through interfaces in EC3 and in PICA (Fig. 1*C*) (18, 19), hindering study of the monomeric protein. Therefore, we introduced a dimerization-disrupting mutation, V250D (18), into EC3 and truncated the protein just before the PICA domain (Fig. 1*D*).

Using a short site-specific anchor at each of the protein's ends, we placed PCDH15 between an immobile 2-μm-diameter glass pedestal bead and a mobile 1-μm-diameter probe bead. Short, stiff anchors were necessary to avoid masking the elastic properties of PCDH15 by those of the anchors (Fig. 1*E*). The probe bead was confined in a weak optical trap whose forward-scattered light we collected to determine the 3D position of the bead with subnanometer spatial resolution and 1-μs temporal resolution (20, 21). A second optical trap, displaced by a few hundred nanometers from the first, served to deliver a force stimulus (Fig. 1*E*). By increasing the trap's stiffness, we could apply forces up to at least 60 pN to the tethered protein.

Cadherin domains manifest a stereotyped, Ig-like Greek key folding motif and are separated from one another by conserved linkers that each bind up to three Ca^{2+} ions in a canonical arrangement (Fig. 1*F*) (22). Ca^{2+} binding is thought to rigidify the linker regions and to stabilize the cadherin domains against force-induced unfolding (23). The Ca^{2+} concentration of the endolymph, the fluid surrounding tip links, varies between different organs and species from tens to hundreds of micromolar (24, 25). Such concentrations are close to the Ca^{2+} dissociation constants for the various binding sites (15, 26), raising the intriguing possibility that nature adjusts the Ca^{2+} concentration to tune the mechanics of tip link cadherins. Therefore, we explored the behavior of tensioned PCDH15 at three Ca^{2+} concentrations: 3 mM, to saturate all binding sites; 20 μM, a concentration that mimics the concentration of Ca^{2+} in the endolymph of the mammalian cochlea (24); and 0 M.

Because structural changes in proteins are stochastic events driven by thermal forces, the rate at which external force is applied can dramatically change the mechanical response. If a protein is pulled too fast, thermal forces do not have sufficient time to cause barrier crossing in the protein's energy landscape before very high external forces are reached. Consequently, the forces at which structural changes occur are artificially elevated

at high loading rates (27). Even in the absence of an acoustic stimulus, tip links experience a constant resting tension (28) that varies with the frequency sensitivity of a hair cell, from 5 pN at 1 kHz to 34 pN at 4 kHz, with possibly even greater tensions at higher frequencies (13). In each tip link, two copies of PCDH15 act in parallel, and each copy assumes one-half of the tension of the entire link, approximately 3 pN up to at least 17 pN. During stimulation from a moderately loud sound, with a 60-dB sound pressure level, a hair bundle is displaced (29) by <10 nm. Such a stimulus stretches the gating springs (12) by up to 1.4 nm, superimposing an oscillation of only a few piconewtons onto the resting tension. Therefore, in our experiments we had to apply slowly changing forces to explore the influence of resting tension on the mechanical properties of PCDH15.

Unless noted otherwise, we applied force ramps to the single molecule tethers at a loading rate of 130 pN·s^{-1} by linearly increasing the spring constant of the stimulus trap (*SI Appendix*, Fig. S1). The dynamic forces during normal hearing at a frequency of 1 kHz vary much faster, at roughly 5,000 pN·s^{-1}. Our loading rate represented a compromise between slow force application and our desire to collect a statistically relevant number of extension-relaxation cycles for each molecule in a reasonable amount of time. For each cycle, we ramped the force up to 60 pN to cover the entire range of physiologically relevant tensions, then returned it at the same rate to a holding level of 2–4 pN. Depending on the Ca^{2+} concentration, we adjusted the holding level and duration to allow the protein to refold domains after many, but not all, cycles. The chosen loading rate likewise led to unfolding events in only a subset of cycles. With these parameter choices, we were able to trap the protein in a given conformational state for several extension-relaxation cycles, allowing us to precisely characterize the mechanics of each state.

Representative examples of individual force-extension relationships for Ca^{2+} concentrations of 3 mM, 20 μM, and 0 M feature hockey stick-like shapes, as expected for the extension of a biopolymer in a heat bath (Fig. 2 *A*–*C*) (30). As we quantify below, this functional shape indicates that entropic effects dominate PCDH15's elastic response. Abrupt, stepwise extensions, or "rips," in the force-extension relationship correspond to structural changes of the protein under force. In contrast to typical single-molecule experiments, under our loading conditions, PCDH15 never fully unfolded during the extension phase of the stimulus; therefore, we frequently observed extensional structural changes even during the relaxation phase of the stimulus (B_U; Fig. 2*B*). For each Ca^{2+} concentration, a set of conformational changes led to a modulated occupation of the force-extension state space, which we visualize by overlapping hundreds of extension-relaxation cycles for one representative molecule apiece (Fig. 2 *D*–*F*).

Conformational Changes. Rips in the force-extension relations at physiological forces suggest that PCDH15 exists in different structural states during hearing. At a saturating Ca^{2+} concentration, the conformational states accessible to the protein are limited; the state-space heatmap reveals only two major configurations (Fig. 2 *A* and *D*). The second of these configurations is further divided into two substates separated by a difference of only a few nanometers in contour length. State 1 reflects the extensibility of fully folded PCDH15 (*SI Appendix*, Note S1). By fitting a polymer model to the force-extension relations for five molecules, we find that state 2 arises from a combination of two classes of conformational changes, leading to mean ± SEM elongations of 4.0 ± 0.2 nm and 15.8 ± 0.7 nm (respectively, distributions of A_U and B_U in Fig. 2*G* and Table 1). The structural origin of these conformational changes is unknown and difficult to determine owing to the large size of the protein; however, was can rule out the unfolding of entire cadherin domains as the origin of the unfolding events. The length of the folded peptide in each of the 11 cadherin domains ranges from 94 to 123 aa, with a mean of 104 residues. At a contour length of 0.39 nm per residue (31), the unfolding of each cadherin domain is expected to augment the contour length by approximately 36 nm, an elongation of 40.6 nm minus 4.5 nm to account for loss of the folded cadherin domain. The observed contour length changes of the elongations A_U and B_U therefore represent protein rearrangements less extreme than the complete unfolding of a cadherin domain. At a saturating Ca^{2+} concentration and physiological forces, we never observed length changes in the wild-type protein compatible with full unfolding.

We next asked whether there are unique structural features in PCDH15 that give rise to the elongations A_U and B_U, or whether several different conformational changes, each with a similar contour length change, underlay the observed distributions. In most of the extension-relaxation cycles, we did not observe more than one of either class of events (*SI Appendix*, Fig. S2). The rare occasions in which several events A_U or B_U were detected in a single trace were not reproducible across trials or protein molecules and thus could be explained as the rupture of nonspecific interactions between the protein and either of the confining surfaces. We conclude that a single, unique structural alteration of PCDH15 is responsible for event A_U, whereas a distinct structural change results in event B_U, precluding the occurrence of several events of either type within the same cycle. Interestingly, the force sensitivity of events A_U is much narrower than that of events B_U (Fig. 2*J*). From these distributions, we determined the statistical dependence of both classes. An event A_U generally follows an event B_U ($P < 0.05$ and $P < 0.1$ for three and two of the five tested molecules, respectively). It is plausible that both structural changes resulted from the same cadherin domain, with elongation B_U leading to a destabilization that facilitated elongation A_U.

We found the protein in state 1 at the beginning of many extension-relaxation cycles and concluded that there is a high probability of refolding of both event A_U and event B_U between cycles. Indeed, we routinely detected refolding events A_F during the relaxation phase of our protocol (Fig. 2 *A* and *G*), but rarely observed refolding events B_F (*SI Appendix*, Fig. S3). The latter events likely occurred only at very low forces, for which the slight shortening was lost in Brownian noise (*SI Appendix*, Fig. S4).

We next reduced the Ca^{2+} concentration to the physiological value of 20 μM and exposed a tethered PCDH15 protein to the same force protocol. The extension-relaxation cycles showed mean conformational changes identical to those of the previously observed classes (A_U: 3.9 ± 0.4 nm; B_U: 15.0 ± 0.6 nm; $n = 8$) (Fig. 2*H*). At this Ca^{2+} concentration, however, an additional class of unfolding events emerged with a mean contour length change of 35 ± 1 nm (C_U in Fig. 2 *B* and *H*), in excellent agreement with the elongation expected for unfolding of an entire cadherin domain (32). At holding forces of 2–4 pN, the refolding of cadherin domains was a slow process and occurred on a time scale of seconds, in line with other proteins that feature Ig-like motifs (33). In some extension-relaxation cycles, we observed the successive unfolding of several cadherin domains (*SI Appendix*, Fig. S5). Because unfolding of any of the 11 extracellular cadherin domains should increase the contour length by a similar amount, we could neither assign unfolding events to particular domains nor elucidate the sequence in which the domains unraveled.

The heatmap of all force-extension relationships originated from a mixture of the unfolding events A_U, B_U, and C_U and their respective refolding events. The contour lengths that gave rise to the annotated states 1–8 (Fig. 2*E*) were a consequence of the unfolding of up to three cadherin domains in series with up to one unfolding event of type B_U. Structural changes of types A_U and A_F, which are clearly visible in the heatmap for a Ca^{2+} concentration of 3 mM as a subdivision of state 2 (Fig. 2*D*), are

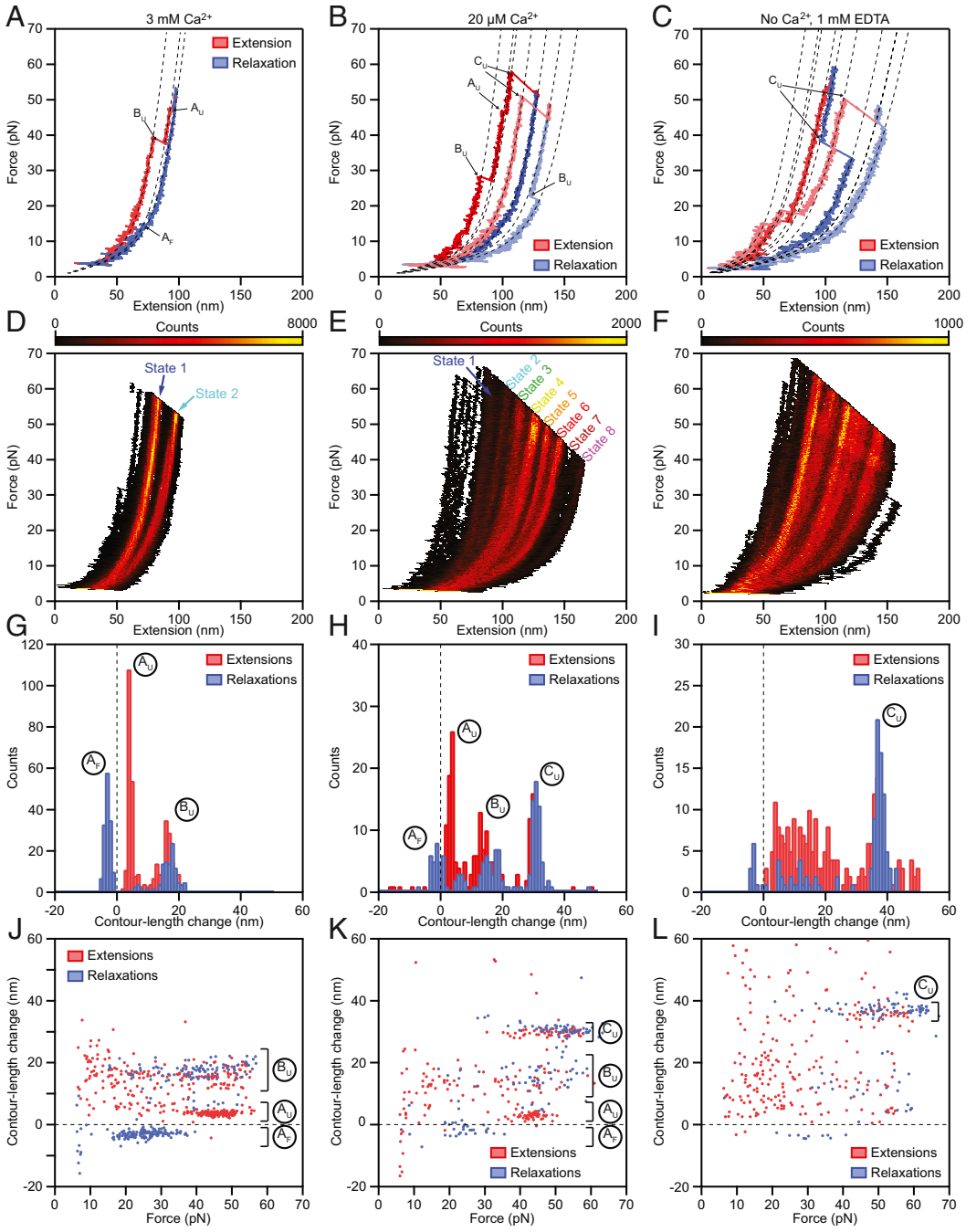

Fig. 2. Force-extension measurements of PCDH15 monomers. (*A*) At a Ca^{2+} concentration of 3 mM, individual force-extension cycles show two distinct classes of abrupt elongations, the unfolding events A_U and B_U, as well as refolding events of class A_F. The dashed lines represent fits to the trajectories by a protein model. (*B*) Reducing the Ca^{2+} concentration to 20 μM elicits an additional class of unfolding events, C_U, corresponding to the unfolding of entire cadherin domains. (*C*) In the absence of Ca^{2+}, unclassifiable structural changes occur in conjunction with the well-defined events C_U. (*D*–*F*) Heatmaps displaying all the force-extension cycles for a single representative molecule at each Ca^{2+} concentration. The data were binned into pixels of 1 nm × 0.1 pN. A much smaller portion of the state space is accessible at a Ca^{2+} concentration of 3 mM than at a Ca^{2+} concentration of 20 μM or in the absence of Ca^{2+}. The heatmaps illustrate which contour lengths of the tethered molecules occurred with increased likelihood during our force-loading protocol as an average over both extensions and relaxations. Prominent regions of elevated occupancy are labeled states 1–8, in which state 1 corresponds to the fully folded protein and state 8 results from the unfolding of three cadherin domains in series with one event of type B_u. (*G*–*I*) Histograms of the contour length changes of all abrupt elongations verify that these rips can be grouped into classes A_F, A_U, B_U, and C_U at Ca^{2+} concentrations of 3 mM and 20 μM. In the absence of Ca^{2+}, most of the contour length changes are more broadly distributed. (*J*–*L*) Plots of the contour length change of every rip against the force at which that event occurred revealing the force distributions of each class of structural change. Note that the extensions never completely unfolded a PCDH15 molecule, so elongations could occur even during the relaxation phases. Because the contour lengths observed for the folded protein correspond to the length of monomeric PCDH15 in series with its molecular anchors, the measured extensions exceed those expected for the protein alone. Our analysis corrects for this influence, resulting in values in excellent agreement with the known structure of the protein (Table 1). All force-extension cycles were sampled at intervals of 10 μs and smoothed to a temporal resolution of 1 ms. The waiting times between cycles were 0.2 s for a Ca^{2+} concentration of 3 mM, 2 s for a Ca^{2+} concentration of 20 μM, and 4 s in the absence of Ca^{2+}. The number of cycles recorded was 500 for a Ca^{2+} concentration of 3 mM and 200 for a Ca^{2+} concentration of 20 μM and in the absence of Ca^{2+}.

Table 1. Material property values of PCDH15

$[Ca^{2+}]$	b, nm	lc_{linker}, nm	k_{folded}, mN/m	Δlc_A, nm	Δlc_B, nm	Δlc_C, nm
3 mM	2.9 ± 0.5	1.4 ± 0.5	9 ± 4	4.0 ± 0.2	15.8 ± 0.7	—
20 μM	3.1 ± 0.4	1.3 ± 0.5	11 ± 5	3.9 ± 0.4	15.0 ± 0.6	35 ± 1

The parameters of a polymer model (*SI Appendix*) were as follows: b, length of each stiff segment of the folded protein; lc_{linker}, contour length of each flexible linker between the stiff segments; k_{folded}, enthalpic stiffness of the folded protein; Δlc_A, contour length increase, type A; Δlc_B, contour length increase, type B; Δlc_C, contour length increase, type C. The parameter values were determined from fits of the model to the force-extension curves in Fig. 2. The values for the folded protein are largely independent of the Ca^{2+} concentration. Δlc_C is in good agreement with the expected contour-length change per unfolded cadherin domain. Fitted parameter values are given as mean ± SEM for five experiments at a Ca^{2+} concentration of 3 mM and for eight experiments at a Ca^{2+} concentration of 20 μM.

not apparent in the state space for a Ca^{2+} concentration of 20 μM. It is possible that there were Ca^{2+}-dependent sub-nanometer changes in the contour length that averaged out small effects of events A_U and A_F in the heatmap. We again investigated a potential sequential dependence of unfolding classes by their force distributions (Fig. 2*K*). Even though events of type A_U followed events of type B_U at a Ca^{2+} concentration of 3 mM, at a physiological Ca^{2+} concentration these structural changes in eight molecules were independent of one another ($P > 0.1$ for each molecule). Moreover, events of types A_U and B_U were independent of events of type C_U, the unfolding of entire cadherin domains.

We next investigated the mechanics of PCDH15 in the absence of Ca^{2+}. Representative force-extension relationships featured a plethora of conformational changes (Fig. 2 *C* and *I*), many of which could no longer be clearly grouped into any of the classes $A_{U,F}$ and B_U. Events with a mean of 37 ± 2 nm (for five molecules) continued to characterize a well-defined class C_U. The heatmap of all extension-relaxation cycles had a structure reminiscent of that at a Ca^{2+} concentration of 20 μM (Fig. 2*F*). The structure in the absence of Ca^{2+} arose from the unfolding of a discrete number of cadherin domains in series with the unclassifiable shorter structural changes that likely represented the partial unfolding of one or more domains. This lack of well-defined short structural changes was also evident from the force distribution of the observed rips (Fig. 2*L*).

Stiffness of PCDH15. It is unknown whether tip link cadherins are completely or only partially folded during normal hearing. Therefore, we investigated the stiffness not only of folded PCDH15, but also that of conformational states with a progressively greater number of unfolded domains. The total stiffness of PCDH15 comprises both enthalpic and entropic components, whose contributions we quantified by fitting the force-extension relationships with a model of the protein. A freely jointed chain (34) formed by the 11 folded cadherin domains, in series with a worm-like chain (35) representing the 10 unstructured linker regions, captured the protein's disorder under tension and reflected its entropic extensibility. The protein's enthalpic extensibility, which likely originates from deformations of its secondary and tertiary structures rather than from unfolding, was modeled through a Hookean spring constant. We included an additional worm-like chain to model any unfolded portions of the protein (*SI Appendix*, Fig. S6).

Because the unfolded polypeptide chains and the linker regions are structurally similar, we modeled both with the same persistence length. Fits to the data for 13 molecules yielded a mean $lp_{peptide}$ value of 0.49 ± 0.04 nm. For folded PCDH15 at a Ca^{2+} concentration of 3 mM, we found a mean length of 2.9 ± 0.5 nm for each of the 11 solid segments of the chain, a mean length of 1.4 ± 0.5 nm for each of the 10 flexible linkers between the solid segments, and a mean enthalpic spring constant of 9 ± 4 $mN \cdot m^{-1}$ for the Hookean stiffness of the protein ($n = 5$ molecules) (Table 1). The full length of a solid segment combined with its associated linker region was 4.3 ± 0.7 nm, in excellent agreement with the value of 4.5 nm per cadherin repeat from crystal structures of cadherin domains (22). Much to our surprise, these values did not change when the Ca^{2+} concentration was decreased to 20 μM, the physiological level in the cochlea. An elevated Ca^{2+} concentration stabilizes cadherin domains against unfolding but does not augment the stiffness of the folded protein. The stiffness predicted by our model is in good agreement with the slopes of the different states in the state-space heatmap (Fig. 3).

Across all states and Ca^{2+} concentrations, the measured and predicted stiffness of the protein is much smaller than its enthalpic stiffness of ∼10 $mN \cdot m^{-1}$. The additional compliance is entropic, arising from the thermal motion of the individual cadherin domains and from thermal undulations in the interdomain linker regions and unfolded polypeptide chains. When PCDH15 is tensed, this thermal kinking is smoothed out, and the protein elongates. The progressive unfolding of domains further softens the protein by introducing additional disordered polypeptide chains (Fig. 3*B*). At high forces, most thermal bends have been straightened, and the enthalpic elasticity begins to dominate the protein's response. Importantly, we find that for physiological tensions, the protein's response to force is determined by entropic elasticity. The protein's stiffness approaches its enthalpic value only for unphysiologically high tensions (Fig. 3 and *SI Appendix*, Fig. S7).

Unfolding of Cadherin Domains Under Forces Relevant for Hearing. Elevated tension not only increases the stiffness of PCDH15, but also increases the likelihood that entire cadherin domains unfold. Do cadherin domains unfold during normal hearing? If so, do they refold under physiological conditions, or could tip links with persistently unstructured regions exist in vivo?

To determine the unfolding rate of cadherin domains under physiological tensions, we transformed the force distributions of type C_U unfolding events into unfolding rates as a function of constant force (Fig. 4) (27). For a given unfolding event, we could not determine which of the 11 cadherin domains had unfolded, so our result is an average over several or all of the domains. The transformation also assumed no cooperativity between the unfolding of individual domains. If the unfolding of one domain were to increase the probability that an adjacent domain would unravel, for example, then our approach would have systematically overestimated the rate at which fully folded tip links unfold.

We computed unfolding rates for Ca^{2+} concentrations of both 20 μM and 0 M (Fig. 4). As expected, the presence of Ca^{2+} stabilized cadherin against force-induced unfolding; the domains unfolded many times faster in the ion's absence than in its presence. With a physiological Ca^{2+} concentration and at 20 pN of tension, the upper range of physiological resting values, a single cadherin domain unfolded at a rate of approximately once every 100 s. A fully folded PCDH15 molecule—consisting of 11 domains—then unfolded a domain every 10 s. At even higher tensions, this rate rapidly increased to roughly 0.4 s^{-1} for the unfolding of a single cadherin domain at a tension of 60 pN. Because unfolding events at forces of 10–20 pN were extremely rare and might have corresponded to transitions from molten-globule states (*SI Appendix*, Note S2), we were unable to reliably calculate force-dependent unfolding rates for this force range. Nevertheless, extrapolation of the available data suggests a rate of ∼0.003 s^{-1} at 10 pN of tension.

These results indicate that unfolding of cadherin domains would not occur within individual cycles of an auditory stimulus. For physiological forces, the unfolding rate is much too low to

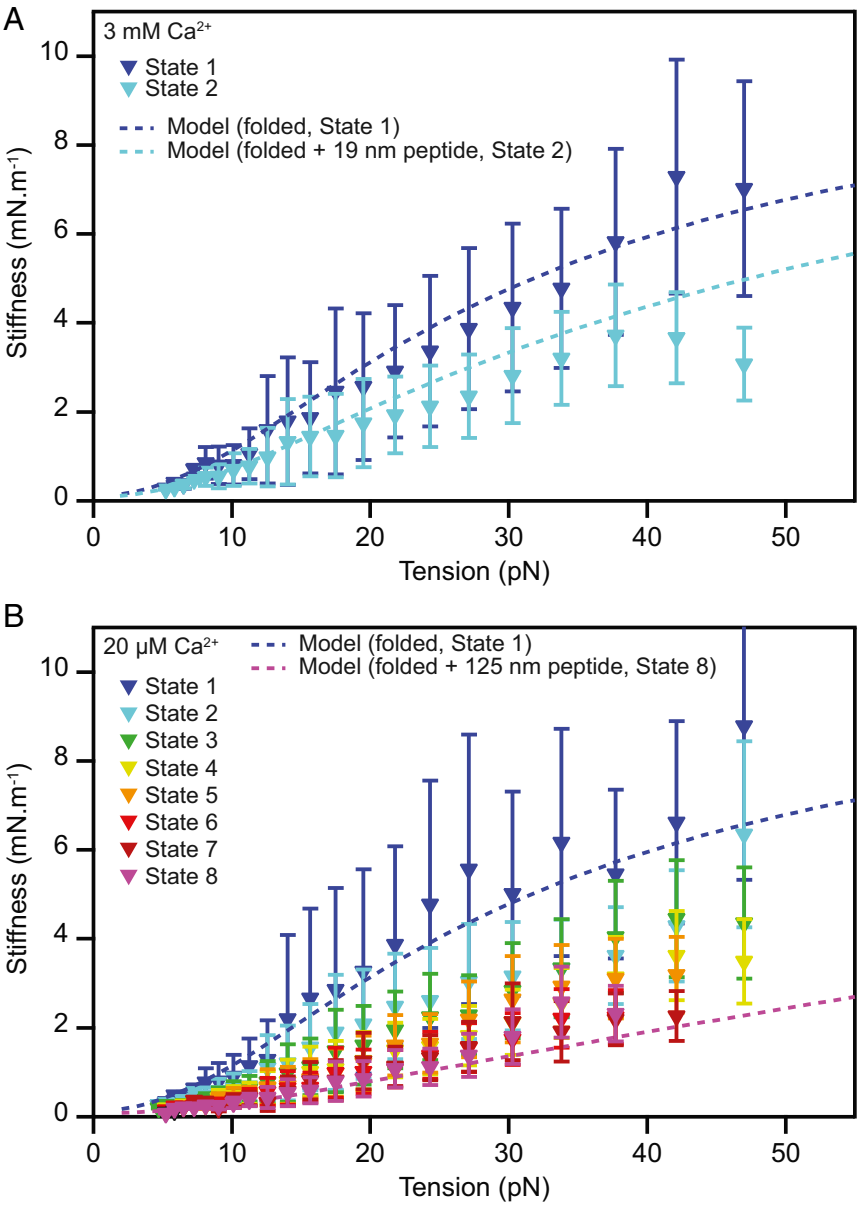

Fig. 3. Stiffness of monomeric PCDH15. (*A*) The stiffnesses of the different conformational states of PCDH15 at a Ca^{2+} concentration of 3 mM correspond to the slopes of the highly occupied regions of the state space in Fig. 2 *D* and *E* and are corrected for the stiffness of the molecular tags and anchors. The dark-blue dashed line represents the stiffness of our model of state 1, the fully folded protein, with the parameter values of Table 1 (b = 3.0 nm; $l_{c_{linker}}$ = 1.35 nm; k_{folded} = 10 mN·m^{-1}). Parameter values were averaged over both Ca^{2+} concentrations. The light-blue dashed line represents the model for state 2, with an additional 19-nm segment of unfolded protein with a persistence length of 0.49 nm representing the combined effect of the events A_U and B_U. (*B*) The corresponding data for a Ca^{2+} concentration of 20 μM capture a variety of unfolding events leading to states 2–8. The dark-blue dashed line represents a model of the fully folded protein (state 1); the pink dashed line depicts the modeled stiffness of the protein in state 8, with an unstructured 125-nm-long peptide to represent the unfolding of three cadherin domains in series with contour length changes of 15 nm and 4 nm. The experimental data are mean ± SEM for five molecules at a Ca^{2+} concentration of 3 mM and for six molecules at a Ca^{2+} concentration of 20 μM.

follow stimuli with frequencies ranging from hundreds to thousands of hertz. However, provided that at the link's resting tension, a domain's unfolding rate exceeds its refolding rate, cadherin domains in a tensed tip link could exist in a permanently unfolded state. We never observed refolding of cadherin domains during any of the recorded extension-relaxation cycles, even though such events should be readily detectable at tensions exceeding 4 pN (*SI Appendix*, Fig. S4). Instead, refolding occurred only during the holding phase between successive cycles, provided that the holding force was <4 pN and the waiting time was on the order of several seconds.

We conclude that for tensions >20 pN per molecule, the unfolding rate—although very small—exceeds the refolding rate. Our data indicate that this is also the case for the force range of 4–20 pN, but owing to the possible influence of molten-globule states, we could not determine this with certainty. Future experiments with force jumps and constant forces might shed light on the existence and behavior of molten-globule states in this force regime. Our result suggests that some cadherin domains of tip links in vivo exist in a perpetually unfolded state. Such unfolded states would decrease the protein's stiffness (Fig. 3*B*) and could be a mechanism by which a tip link softens even under high tension.

The critical force at which the unfolding and refolding rates of a cadherin domain are equal remains to be determined. However, the giant muscle protein titin, which has immunoglobin folds similar to those of cadherin, exhibits a critical force of 5.4 pN (33). If cadherin domains feature a similar value, the resting tensions in low-frequency hair cells might be less than the critical force and bias the tip link's domains toward a fully folded state, whereas the tip link might remain in a partially unfolded state in hair cells sensitive to high frequencies.

Effect of a Mutation Associated with Hearing Loss. More than 100 mutations of the tip link cadherins cause hearing loss in humans (36). The deletion of residue V767 in EC7 (Fig. 5*A*) is of particular interest, for it leads to deafness—stemming from a deficit in the cochlea, with its low Ca^{2+} concentration—but not loss of function in the vestibular labyrinth, which has a higher Ca^{2+} concentration (37). This mutation evidently does not hinder

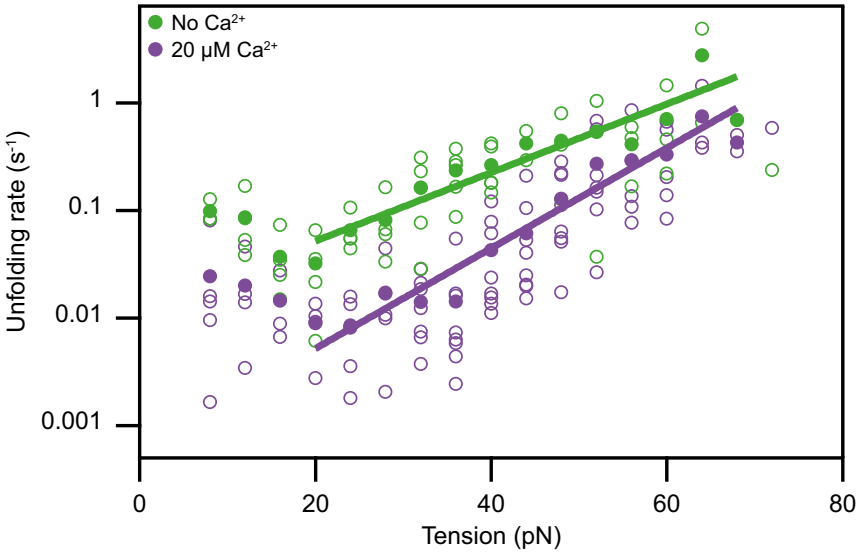

Fig. 4. Tension-dependent unfolding rates of a single cadherin domain. Assuming that all domains of PCDH15 are similar and unfold independently, we estimate the rate at which individual EC domains unfold as a function of tension. Domains unfold much more readily in the absence of Ca^{2+} (green) than at a physiological Ca^{2+} concentration of 20 μM (purple). The filled circles represent the means for eight molecules at a Ca^{2+} concentration of 20 μM and for five molecules in the absence of Ca^{2+}. The outlined circles, which represent the data for individual molecules, provide an estimate of the data's spread. The solid lines are fits of Bells' model (48) to the data. For 20 μM Ca^{2+}, the unfolding rate with no force is $k_0 = 0.0006 \pm 0.0002\ s^{-1}$, and the transition-state distance is $x^{\ddagger} = 0.44 \pm 0.04$ nm; in the absence of Ca^{2+}, these values are $k_0 = 0.012 \pm 0.006\ s^{-1}$ and $x^{\ddagger} = 0.30 \pm 0.04$ nm.

tip link formation, but it might change the elastic properties of the link.

We investigated how this deletion affects the mechanical properties of monomeric PCDH15 (V250D, ΔV767) and found a small but detectable probability that force unfolded a complete cadherin domain even when PCDH15 was saturated with Ca^{2+} (Fig. 5*B*). During identical treatment of Ca^{2+}-saturated proteins without pathological mutations, we never observed the unfolding of complete domains (Fig. 2*G*). By shortening one strand of EC7, the mutation likely caused a slight misalignment of amino acid residues and thus destabilized the domain. When we performed experiments at the physiological Ca^{2+} concentration of 20 μM, we could not detect a difference in domain unfolding between the mutant and wild-type proteins.

Discussion

The behavior of a gated ion channel is usually binary: the channel is open or closed. Nevertheless, a mechanically activated channel can signal fine nuances of a stimulus by rapidly fluttering between the two states, such that the average open probability provides a smoothly graded representation of the stimulus. A gating spring makes this possible. Tensed by a stimulus and battered by thermal noise, the spring continuously adjusts the open probability of the associated channel over a significant range of inputs. This range is determined by the gating spring's stiffness, and thus by such molecular details as the entropic elasticity and folding transitions demonstrated here.

The stiffness of gating springs in outer hair cells increases with increased resting tension along the tonotopic axis (13), from 1.3 $mN{\cdot}m^{-1}$ at 5 pN of tension to 3.7 $mN{\cdot}m^{-1}$ at 34 pN. Simulations of short segments of tip link proteins found that they are orders of magnitudes too stiff to account for these values (15, 38). However, our single-molecule experiments on the extracellular domain of PCDH15 show that the protein has a stiffness comparable to that of gating springs in vivo and displays similar strain-hardening. Across the physiological force range, most of PCDH15's compliance is of entropic origin; the protein's enthalpic stiffness of 10 $mN{\cdot}m^{-1}$ emerges only at very high tension. Our stiffness values (Fig. 3) are systematically lower than those found for gating springs in vivo, which is not surprising because our measurements tested only a monomer of one constituent protein. The dimeric arrangement of PCDH15 roughly doubles the enthalpic stiffness of the monomer. Moreover, a tip link adopts a helical structure (14, 18) that likely reduces the magnitude of its thermal undulations, decreasing the entropic contribution to the tip link's mechanics and further

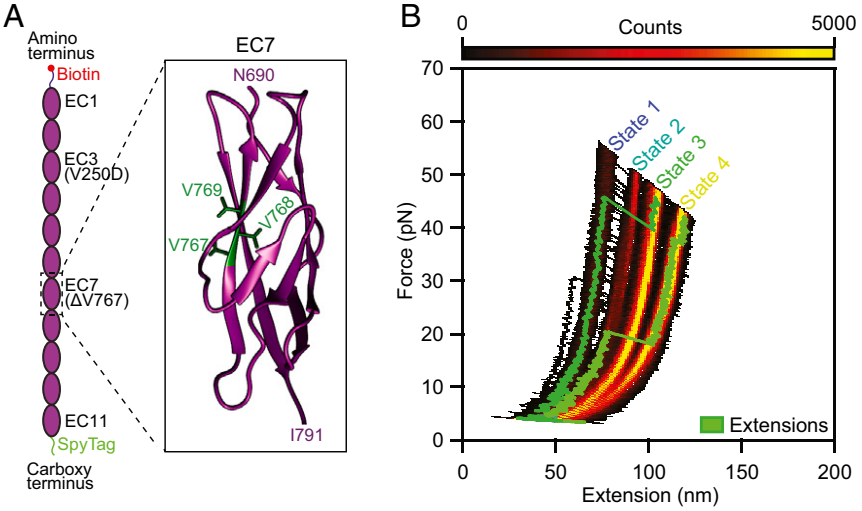

Fig. 5. Effect of a hearing loss-associated mutation on PCDH15 mechanics. (*A*) We deleted V767 in the seventh EC domain of PCDH15. As indicated in the crystal structure (Protein Data Bank ID code 5W1D; image generated with UCSF Chimera), V767 is located in the F strand of the cadherin fold. (*B*) A state-space heatmap for 500 extension-relaxation cycles reveals that at a Ca^{2+} concentration of 3 mM the mutant protein can assume four distinct conformational states. The two additional states not observed in the wild-type protein result from unfolding of the pathological cadherin domain in series with the usual states 1 and 2. Unfolding of the pathological domain is rare and occurs in only a few cycles, two of which are superimposed on the heat map (green traces). The waiting time between cycles was 0.2 s.

increasing its stiffness. Finally, the arrangement of a dimer of CDH23 in series with the PCDH15 dimer is expected to reduce the stiffness by approximately 70%. At very high tensions, when entropic effects are largely suppressed and enthalpy dominates, we estimate the stiffness of the full-length, dimeric tip link as 6 $mN \cdot m^{-1}$ (*SI Appendix*, Note S3), a value in good agreement with the stiffness of strongly tensioned gating springs in vivo (13). Provided that entropy further softens the tip link at lower tensions, our results suggest that the tip link cadherins are a major component of the gating spring for mechanotransduction in hair cells. The entropic contributions to the mechanics of dimeric PCDH15 and of the entire tip link remain to be determined.

The stiffness of hair bundles has a complicated, nonmonotonic dependence on Ca^{2+} concentration (39, 40), an observation that may be interpreted as the interplay between strain-hardening of the tip links and the unfolding of cadherin domains. Low Ca^{2+} levels cause molecular motors to up-regulate tip link tension (41), which suppresses each link's thermal motion and increases its stiffness. Ca^{2+} also directly affects the rate at which cadherin domains unfold under force, however, resulting in states of PCDH15 with reduced stiffness (Fig. 3). At a tension of 20 pN and a Ca^{2+} concentration of 20 μM, individual cadherin domains unfold an order of magnitude more slowly than in the absence of Ca^{2+}. We never observed the unfolding of entire cadherin domains at a Ca^{2+} concentration of 3 mM. Thus, the Ca^{2+} concentration regulates both the tension on and the structure of PCDH15, the combined effect of which on the molecule's mechanics is hard to predict. Nevertheless, the sensitivity of PCDH15 to Ca^{2+} suggests that the variable concentrations of the ion in different receptor organs tunes the mechanical properties of tip links, and thus of hair bundles, to the organs' specific requirements. Even within a single organ, the guinea pig cochlea, the Ca^{2+} concentration increases fourfold along the tonotopic axis from base to apex (25). This gradient might adjust tip link stiffness to accord with the frequency response of the individual hair cells. Finally, hair cells can enhance the local Ca^{2+} concentration around their hair bundles through the activity of membrane Ca^{2+} pumps (42). This phenomenon raises the interesting possibility that the stiffness of tip links is modulated by the locally varying Ca^{2+} concentration in response to hair cell activity.

We found that the elastic properties of folded PCDH15 are surprisingly independent of the Ca^{2+} concentration. This result seems to contradict the impression conveyed by electron micrographs (43), in which cadherins transition from a disordered globular conformation to a rod-like chain of domains in the presence of progressively larger amounts of Ca^{2+}. Disordered states should make greater entropic contributions to PCDH15's elasticity than ordered states, a difference not apparent in our data. Note, however, that the divergence between electron-microscopic images and single-molecule data has also been observed for other proteins, such as titin (44). A possible explanation is that the configurations of proteins adsorbed to substrates are far from their equilibrium conformations, so that the variations in shape do not accurately capture the thermal motion in solution (45).

The displacement-transduction current relationships of hair bundles reveal that for unphysiologically large displacements in excess of 1 μm, gating springs can stretch (46) by at least 120 nm, a value thought to be incompatible with the extensibility of tip link cadherins. Consequently, it has been suggested that the gating spring's stiffness stems from the elasticity of the plasma membrane or cytoskeleton into which the tip links insert (47). We have shown that invoking such sources of elasticity is unnecessary; cadherin domains in the tip link proteins can unfold under physiological stimuli, albeit at a low rate, and such unfolding events become very likely at high forces. Recall that physiological hair bundle displacements are on the order of 10 nm and augment the resting tension of each tip link by a few piconewtons. The stimulus in extreme deflections, which is 100-fold greater, is capable of causing the almost instantaneous unfolding of individual cadherin domains. Several unfolded cadherin domains could then account for the extreme tip link elongation of 120 nm.

In further support of domain unfolding, the length distribution of tip links in the bullfrog's hair bundles, as determined by electron-microscopic tomography, features two distinct classes (10) with means close to 110 nm and 170 nm. The unfolding of two cadherin domains per tip link monomer could account for this length difference. Such unfolding events could soften the gating spring at high resting tensions and protect both the tip link and the associated mechanotransduction machinery from damage during loud sounds.

In addition to the unfolding of entire cadherin domains, we also observed partial domain unfolding with contour length increases of 4 nm and 15 nm. Future single-molecule work is needed to elucidate the structural correlates of these conformational changes and to determine their role in hearing. Additional experiments are also needed to test the stiffness of PCDH15 dimers and of the full tip link and to confirm that domain unfolding occurs for those constructs and for tip links in vivo.

Methods

More detailed information is provided in *SI Appendix, Materials and Methods*.

Preparation of PCDH15 Monomers. Plasmids encoding murine PCDH15 were expressed in suspension-adapted HEK293 cells. To confine monomers in an optical trap, the amino terminus of the protein was labeled with an AviTag that permitted the enzymatic conjugation of biotin. The carboxyl terminus included a SpyTag that could form a covalent linkage with an immobilized SpyCatcher protein. The construct also encoded a signal peptide to promote secretion, short flexible linkers flanking the PCDH15 sequence, and a His tag for purification.

Optical Trapping and Measurements. SpyCatcher molecules were conjugated to 2-μm silicon dioxide pedestal beads that were covalently attached to a glass coverslip. PCDH15 monomers were washed into the sample chamber and allowed to attach covalently to the pedestal beads. To initiate an experiment, we optically trapped a streptavidin-coated 1-μm polystyrene bead and positioned it near a pedestal bead. Using a highly focused 852-nm laser beam, we applied stimulus forces to probe the molecule's mechanical properties. With a second, high-stability 1,064-nm laser, we monitored the position of the probe bead with a precision of ≤1 nm in each of three dimensions.

ACKNOWLEDGMENTS. We thank Julio Fernandez and Jaime Andrés Rivas-Pardo for guidance concerning the chemical functionalization of glass substrates, Brian Fabella and Vadim Sherman for high-precision fabrication, Brandon Razooky and Maria Vologodskaia for assistance with cloning, and Anna Kaczynska for help with protein expression. The crystal structure in Fig. 5 was deposited by Carissa Klanseck, Brandon Neel, and Marcos Sotomayor. F.E.H. acknowledges financial support by the Studienstiftung des Deutschen Volkes. A.O. was supported by the Medical Research Fellows Program of Howard Hughes Medical Institute. T.F.B. was partially supported by a Junior Fellow award from the Simons Foundation and a Pilot Grant from the Kavli Foundation. A.J.H. is an Investigator of Howard Hughes Medical Institute.

1. Wiggins P, Phillips R (2004) Analytic models for mechanotransduction: Gating a mechanosensitive channel. *Proc Natl Acad Sci USA* 101:4071–4076.
2. Saotome K, et al. (2018) Structure of the mechanically activated ion channel Piezo1. *Nature* 554:481–486.
3. Zhao Q, et al. (2018) Structure and mechanogating mechanism of the Piezo1 channel. *Nature* 554:487–492.
4. Jin P, et al. (2017) Electron cryo-microscopy structure of the mechanotransduction channel NOMPC. *Nature* 547:118–122.
5. Corey DP, Hudspeth AJ (1983) Kinetics of the receptor current in bullfrog saccular hair cells. *J Neurosci* 3:962–976.
6. Hudspeth AJ (2014) Integrating the active process of hair cells with cochlear function. *Nat Rev Neurosci* 15:600–614.

7. Reichenbach T, Hudspeth AJ (2014) The physics of hearing: Fluid mechanics and the active process of the inner ear. *Rep Prog Phys* 77:076601.
8. Pickles JO, Comis SD, Osborne MP (1984) Cross-links between stereocilia in the guinea pig organ of Corti, and their possible relation to sensory transduction. *Hear Res* 15: 103–112.
9. Assad JA, Shepherd GM, Corey DP (1991) Tip-link integrity and mechanical transduction in vertebrate hair cells. *Neuron* 7:985–994.
10. Auer M, et al. (2008) Three-dimensional architecture of hair-bundle linkages revealed by electron-microscopic tomography. *J Assoc Res Otolaryngol* 9:215–224.
11. Sotomayor M, Weihofen WA, Gaudet R, Corey DP (2012) Structure of a force-conveying cadherin bond essential for inner-ear mechanotransduction. *Nature* 492: 128–132.
12. Howard J, Hudspeth AJ (1988) Compliance of the hair bundle associated with gating of mechanoelectrical transduction channels in the bullfrog's saccular hair cell. *Neuron* 1:189–199.
13. Tobin M, Chaiyasitdhi A, Michel V, Michalski N, Martin P (2019) Stiffness and tension gradients of the hair cell's tip-link complex in the mammalian cochlea. *eLife* 8:e43473.
14. Kachar B, Parakkal M, Kurc M, Zhao Y, Gillespie PG (2000) High-resolution structure of hair-cell tip links. *Proc Natl Acad Sci USA* 97:13336–13341.
15. Sotomayor M, Weihofen WA, Gaudet R, Corey DP (2010) Structural determinants of cadherin-23 function in hearing and deafness. *Neuron* 66:85–100.
16. Albert JT, Kozlov AS (2016) Comparative aspects of hearing in vertebrates and insects with antennal ears. *Curr Biol* 26:R1050–R1061.
17. Smith SB, Finzi L, Bustamante C (1992) Direct mechanical measurements of the elasticity of single DNA molecules by using magnetic beads. *Science* 258:1122–1126.
18. Dionne G, et al. (2018) Mechanotransduction by PCDH15 relies on a novel cis-dimeric architecture. *Neuron* 99:480–492.e5.
19. Ge J, et al. (2018) Structure of mouse protocadherin 15 of the stereocilia tip link in complex with LHFPL5. *eLife* 7: e38770.
20. Pralle A, Prummer M, Florin E-L, Stelzer EHK, Hörber JK (1999) Three-dimensional high-resolution particle tracking for optical tweezers by forward scattered light. *Microsc Res Tech* 44:378–386.
21. Bartsch TF, Kochanczyk MD, Lissek EN, Lange JR, Florin E-L (2016) Nanoscopic imaging of thick heterogeneous soft-matter structures in aqueous solution. *Nat Commun* 7: 12729.
22. Shapiro L, et al. (1995) Structural basis of cell-cell adhesion by cadherins. *Nature* 374: 327–337.
23. Nagar B, Overduin M, Ikura M, Rini JM (1996) Structural basis of calcium-induced E-cadherin rigidification and dimerization. *Nature* 380:360–364.
24. Bosher SK, Warren RL (1978) Very low calcium content of cochlear endolymph, an extracellular fluid. *Nature* 273:377–378.
25. Salt AN, Inamura N, Thalmann R, Vora A (1989) Calcium gradients in inner ear endolymph. *Am J Otolaryngol* 10:371–375.
26. Powers RE, Gaudet R, Sotomayor M (2017) A partial calcium-free linker confers flexibility to inner-ear protocadherin-15. *Structure* 25:482–495.
27. Zhang Y, Dudko OK (2013) A transformation for the mechanical fingerprints of complex biomolecular interactions. *Proc Natl Acad Sci USA* 110:16432–16437.
28. Jaramillo F, Hudspeth AJ (1993) Displacement-clamp measurement of the forces exerted by gating springs in the hair bundle. *Proc Natl Acad Sci USA* 90:1330–1334.
29. Chen F, et al. (2011) A differentially amplified motion in the ear for near-threshold sound detection. *Nat Neurosci* 14:770–774.
30. Marko JF, Siggia ED (1994) Fluctuations and supercoiling of DNA. *Science* 265:506–508.
31. Ainavarapu SRK, et al. (2007) Contour length and refolding rate of a small protein controlled by engineered disulfide bonds. *Biophys J* 92:225–233.
32. Oroz J, et al. (2011) Nanomechanics of the cadherin ectodomain: "canalization" by Ca^{2+} binding results in a new mechanical element. *J Biol Chem* 286:9405–9418.
33. Chen H, et al. (2015) Dynamics of equilibrium folding and unfolding transitions of titin immunoglobulin domain under constant forces. *J Am Chem Soc* 137:3540–3546.
34. Rubinstein M, Colby RH (2003) *Polymer Physics* (Oxford Univ Press, Oxford).
35. Marko JF, Siggia ED (1995) Stretching DNA. *Macromolecules* 28:8759–8770.
36. Jaiganesh A, et al. (2018) Zooming in on cadherin-23: Structural diversity and potential mechanisms of inherited deafness. *Structure* 26:1210–1225.e4.
37. Zhan Y, Liu M, Chen D, Chen K, Jiang H (2015) Novel mutation located in EC7 domain of protocadherin-15 uncovered by targeted massively parallel sequencing in a family segregating non-syndromic deafness DFNB23. *Int J Pediatr Otorhinolaryngol* 79:983–986.
38. Sotomayor M, Corey DP, Schulten K (2005) In search of the hair-cell gating spring elastic properties of ankyrin and cadherin repeats. *Structure* 13:669–682.
39. Marquis RE, Hudspeth AJ (1997) Effects of extracellular $Ca2^{+}$ concentration on hair-bundle stiffness and gating-spring integrity in hair cells. *Proc Natl Acad Sci USA* 94: 11923–11928.
40. Tinevez J-Y, Jülicher F, Martin P (2007) Unifying the various incarnations of active hair-bundle motility by the vertebrate hair cell. *Biophys J* 93:4053–4067.
41. Bechstedt S, Howard J (2007) Models of hair cell mechanotransduction. *Mechanosensitive Ion Channels, Part B*. Current Topics in Membranes, eds Simon S, Bemos D (Academic, New York), Vol 59, pp 399–424.
42. Yamoah EN, et al. (1998) Plasma membrane $Ca2^{+}$-ATPase extrudes $Ca2^{+}$ from hair cell stereocilia. *J Neurosci* 18:610–624.
43. Kazmierczak P, et al. (2007) Cadherin 23 and protocadherin 15 interact to form tip-link filaments in sensory hair cells. *Nature* 449:87–91.
44. Leake MC, Wilson D, Gautel M, Simmons RM (2004) The elasticity of single titin molecules using a two-bead optical tweezers assay. *Biophys J* 87:1112–1135.
45. Broedersz CP, MacKintosh FC (2014) Modeling semiflexible polymer networks. *Rev Mod Phys* 86:995–1036.
46. Shepherd GM, Corey DP (1994) The extent of adaptation in bullfrog saccular hair cells. *J Neurosci* 14:6217–6229.
47. Powers RJ, et al. (2012) Stereocilia membrane deformation: Implications for the gating spring and mechanotransduction channel. *Biophys J* 102:201–210.
48. Bell GI (1978) Models for the specific adhesion of cells to cells. *Science* 200:618–627.